NANO LETTERS

Letter

pubs.acs.org/NanoLett

Resonant Electronic Coupling Enabled by Small Molecules in Nanocrystal Solids

Rui N. Pereira,*[,†,‡] José Coutinho,*[,†] Sabrina Niesar,[‡] Tiago A. Oliveira,[†] Willi Aigner,[‡] Hartmut Wiggers,[§] Mark J. Rayson,[∥] Patrick R. Briddon,[⊥,#] Martin S. Brandt,[‡] and Martin Stutzmann[‡]

[†]Department of Physics and I3N, University of Aveiro, Campus Universitário de Santiago, 3810-193 Aveiro, Portugal

[‡]Walter Schottky Institut and Physik-Department, Technische Universität München, Am Coulombwall 4, 85748 Garching, Germany

[§]Institut für Verbrennung und Gasdynamik and CENIDE, Universität Duisburg-Essen, 47048 Duisburg, Germany

[∥]Department of Chemistry, University of Surrey, Guildford GU2 7XH, United Kingdom

[⊥]Institut des Matériaux Jean Rouxel (IMN), Université de Nantes, CNRS UMR 6502, F-44322 Nantes, France

Supporting Information

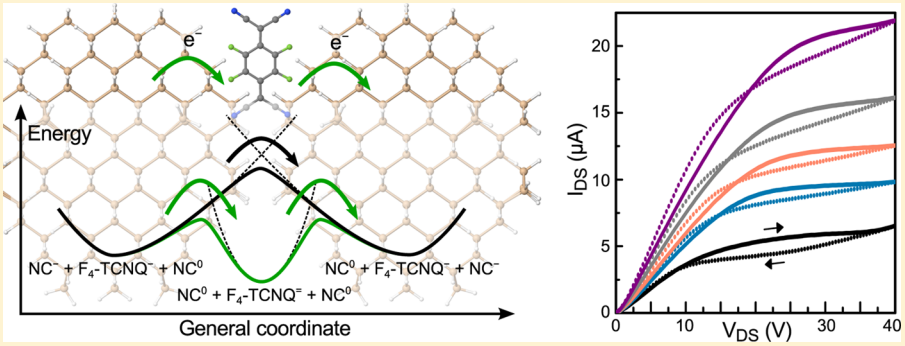

ABSTRACT: The future exploitation of the exceptional properties of nanocrystal (NC) thin films deposited from liquid dispersions of nanoparticles relies upon our ability to produce films with improved electrical properties by simple and inexpensive means. Here, we demonstrate that the electronic conduction of solution-processed NC films can be strongly enhanced without the need of postdeposition treatments, via specific molecules adsorbed at the surfaces of adjacent NCs. This effect is demonstrated for Si NC films doped with the strong molecular oxidizing agent tetrafluoro-tetracyanoquinodimethane (F_4-TCNQ). Density functional calculations were carried out with molecule-doped superlattice solid models. It is shown that, when populated by electrons, hybrid molecule/NC states edge (and may actually resonate with) the conduction-band states of the NC solid. This provides extra electronic connectivity across the NC network as the molecules effectively flatten the electronic potential barriers for electron transfer across the otherwise vacuum-filled network interstitialcies.

KEYWORDS: *Semiconductor nanocrystals, charge transport, electronic coupling, field-effect transistor*

Freestanding nanocrystals (NCs) of inorganic semiconductor materials hold promise for new (opto)electronic applications that take advantage of their size- and shape-tunable optical and electronic properties.[1−16] Such NCs are attractive also from a processing perspective. Liquid dispersions of NCs (NC inks) can be used for low-cost, print-type deposition of semiconductors,[7,17−23] as opposed to the conventional and more costly vacuum deposition methods. Besides allowing for patterning devices onto large-area and flexible substrates,[24−26] solution-based deposition protocols and the freestanding nature of the NCs open the possibility of controlling the specifics of the NC surface, enabling a great deal of flexibility in selecting and controlling the inter-NC medium. NC-based materials have been proposed for many technologies, including thin-film field-effect transistors (FETs),[23,26,27] photodetectors,[28−32] photovoltaics,[29,33−42] thermoelectrics,[43] and light-emitting diodes.[44,45] However, the relatively inefficient electrical transport associated with nanoparticulate solids[46,47] has challenged the scientific community to improve the electronic charge transport across NC films (NC solids) with the goal of enabling their widespread utilization.

In CdX and PbX (X = S, Se, Te) NCs, long-chain organic capping ligands, typically acquired during the chemical synthesis and schematically shown in Figure 1a,[7,48] prevent the close proximity between NCs in NC solids. Hence, inter-NC charge transfer (CT), and consequently long-range carrier transport, are heavily inhibited due to the high and wide configurational energy barriers involved. A configuration coordinate diagram with such an intrinsic barrier is schemati-

Received: March 12, 2014
Revised: May 14, 2014
Published: May 21, 2014

   dx.doi.org/10.1021/nl500932q | *Nano Lett.* 2014, 14, 3817−3826

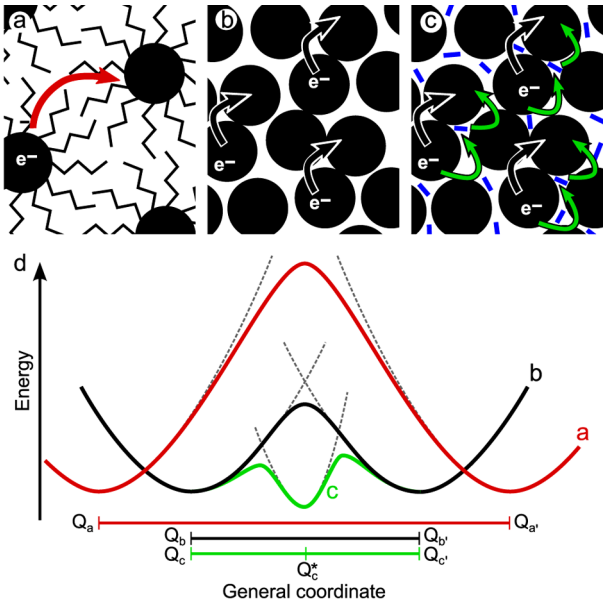

Figure 1. Schematic comparison between CT paths that may take place across networks of (a) NCs with long surface ligands, (b) NCs with ultrasmall (or without) surface ligands, and (c) NCs with ultrasmall surface ligands and mixed with CT mediating molecules. Black circles, zigzag chains, and blue ribbons represent the nanocrystals, surface ligands, and CT mediating molecules, respectively. (d) Depicts configuration coordinate diagrams suggesting transition barriers for inter-NC CT in NC networks as depicted in (a) $Q_a \leftrightarrow Q_{a'}$, in (b) $Q_b \leftrightarrow Q_{b'}$, and in (c) $Q_c \leftrightarrow Q_{c'}$.

cally represented by the potential energy surface "a" in Figure 1d. A great deal of research has been carried out in recent years to develop ways to replace these long and bulky ligands by shorter ligands, including molecular metal chalcogenide complexes,[49,50] chalcogenide ions,[51] thiocyanate,[52−54] halides,[39] and trialkyl oxonium.[55] The application of some of the ligand-exchange procedures developed for CdX and PbX (X = S, Se, Te) NCs subsequently led to the report of record performance NC-based FETs[52,54,56,57] and photovoltaic devices.[39]

Despite achieving more compact NC networks with the help of ultrasmall ligands, these recipes alone will not ensure an optimized charge transport. The large fraction of empty space within such materials (see Figure 1b) still poses major limitations to efficient CT. That is, although closing the separation between NCs may reduce barrier heights and widths, as suggested by the potential energy surface "b" in Figure 1d, CT is still limited by the low (or even vanishing) local density of states in the large empty space regions that are characteristic for such granular materials. In this respect, new routes toward improving inter-NC electronic coupling, ideally disposed of postdeposition treatments with high yield and production-line-ready, are definitely needed.

The present work combines experimental and theoretical investigations to demonstrate that inter-NC electronic coupling in NC solids can effectively be enhanced by specific molecules adsorbed at the surfaces of adjacent NCs. These molecules are conveniently introduced in the NC films without postdeposition treatment by simply doping the film-forming NC inks with a small amount of the corresponding substance. The utility of this method is demonstrated for Si NCs, where the NC surface termination with ultrasmall ligands (Si−H bonds) is rather well understood, controllable, and easily obtainable. In thin-films of H-terminated Si NCs, neighboring NCs are already in almost direct contact. For these reasons, these films provide an ideal model system to find inter-NC coupling effects beyond the recipes based on increasing the inter-NC proximity,[39,49−55,58] which are ultimately limited by the NCs shape.

Si NCs are in their own right also very interesting from the technological point of view,[5,36,59−65] offering important benefits over the more traditional CdX and PbX (X = S, Se, Te) NCs.[27,56,66,67] These include the nontoxicity and high natural abundance of silicon as well as the massive Si-based microelectronics technological background. Presently, high quality (low defect content), size-controlled, and H-terminated Si NCs can be produced in very large quantities and at low cost by means of plasma-induced decomposition of silane.[4,68,69] We show that the introduction of tetrafluoro-tetracyanoquinodimethane (F_4-TCNQ) molecules as inter-NC coupling agent in Si NC films results in an electrical conductance improvement of up to 2 orders of magnitude in comparison to undoped Si NC films. This molecule was chosen due to its high electron affinity and its ability to accept electrons from high-lying states localized on nearby NCs.[70] We demonstrate that FETs fabricated from solution-processed Si NC layers activated with F_4-TCNQ exhibit the characteristic behavior expected for such thin-film transistors with a linear regime at small drain-source voltages followed by a saturation at higher voltages, minimal hysteresis, and a field-effect electron mobility significantly above the range of values reported so far for the best solution-cast Si NC FETs.[71,72]

We complement the experimental studies with density functional calculations of models of NC solids. We use NC arrays packed in three dimensions to form a periodic superlattice (SL) structure. We show that F_4-TCNQ molecules within the SL interstitialcies introduce empty electronic states that bridge and overlap neighboring NCs, providing extra electronic connectivity to the NC network. The effect is schematically depicted in Figure 1c,d (potential energy surface "c"), indicating that the molecules reduce the effective inter-NC energy barrier heights/widths by introducing intermediate states, otherwise absent in undoped films.

Methods. *Experimental.* The Si NCs used in this study were synthesized by microwave-induced decomposition of silane.[4] With this method, we produced H-terminated (intrinsic) silicon NCs with mean diameters $d_{as-grown}$ chosen in the range of 7−20 nm, as determined by the Brunauer−Emmet−Teller (BET) method,[74] by adjusting the gas flow, the pressure, and the relative concentrations of the precursor gases SiH_4, Ar, and H_2.[4] An example of the X-ray diffraction (XRD) pattern measured for a sample of silicon NCs with mean diameter of 18.5 nm is given in Figure 2a, showing the typical peaks of crystalline silicon. The NCs are crystalline and spherical in shape. The mean diameter of the as-grown NCs obtained from BET method, from XRD patterns, and from transmission electron microscopy images are found to be equal within a deviation of 10%.[75] After synthesis, the NCs were stored in air while an amorphous surface oxide layer is formed with a thickness of 1.4 ± 0.2 nm.[60] The Fourier-transform infrared (FTIR) spectrum recorded with surface-oxidized NCs with $d_{as-grown}$ = 7.0 nm is shown in Figure 2b, confirming the formation of the native oxide shell.[73] A transmission electron microscopy image of the same sample is shown in the inset of Figure 2a, where the crystalline core and the amorphous oxide shell of the NCs can be distinguished. To replace this oxide shell with an H-termination, we used a simple procedure,

dx.doi.org/10.1021/nl500932q | Nano Lett. 2014, 14, 3817−3826

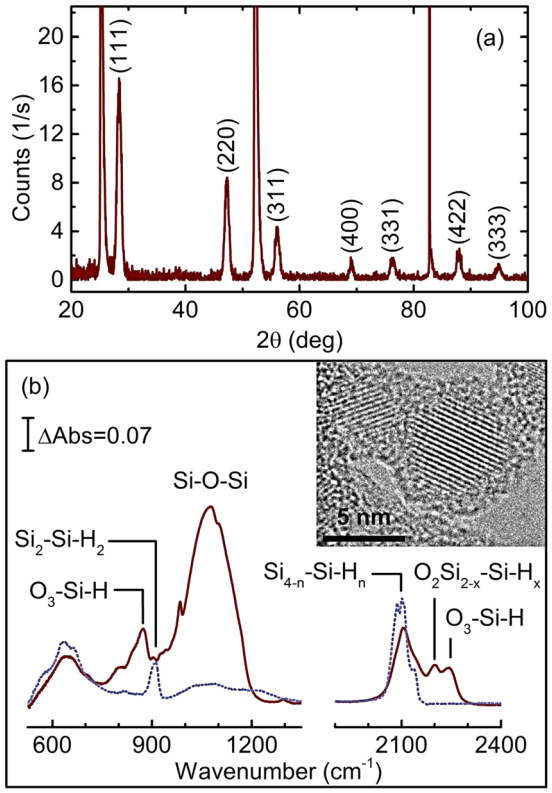

Figure 2. (a) XRD pattern of a sample of silicon NCs with $d_{as-grown}$ = 18.5 nm. The labeled peaks correspond to crystalline silicon and the other are due to the sapphire substrate used for the measurements. (b) FTIR spectrum in the frequency regions of vibrational modes of Si−H and Si−O−Si bonds recorded for a sample of silicon NCs ($d_{as-grown}$ = 7.0 nm) with a native oxide shell (solid line). The inset shows a transmission electron microscopy image of NCs from the same sample. The spectrum shows a strong band in the region 950−1200 cm^{-1} due to Si−O−Si bonds (stretching), together with lines at 2250 and 2200 cm^{-1} due to Si−H stretching modes in O_3−Si−H and O_2H_{2-x}−Si−H_x (x = 1,2) bonds, respectively, and a band at 875 cm^{-1} due to Si−H wagging modes of O_3−Si−H, all related to the surface oxide.[73] A band due to Si_{4-n}−Si−H_n hydrides is also present, as it is typically observed for Si NCs with a native oxide shell.[73] The spectrum recorded for the same NCs after HF etching is also shown (dotted line). This spectrum is dominated by bands at 910 and ∼2100 cm^{-1} due to modes from surface Si_2−Si−H_2 (scissor and wag) and Si_{4-n}−Si−H_n (stretching) bonds.[73]

described previously,[61] that is based on surface etching in diluted HF (10% in water) for 3 min followed by rinsing with ethanol. Figure 2b shows the FTIR spectrum recorded after HF-etching for the case of silicon NCs with $d_{as-grown}$ = 7.0 nm, which confirms that these are terminated with Si−H bonds in the form of Si_{4-n}−Si−H_n (n = 1, 2, 3) surface hydride groups with only a small amount of Si−O−Si bonds remaining. The average diameter d_{NC} of the resulting H-terminated Si NCs, which were used to carry out our study, corresponds to the diameter of the as-grown NCs determined by BET, minus twice the average thickness (1.4 nm) of the native oxide shell. The resulting H-terminated freestanding Si NCs were inserted into an Ar-purged glovebox, with a residual content of oxygen and water below 1 ppm, where further processing was carried out. To produce the NC inks, we dispersed the Si NCs by ultrasonicating a mixture of 5 wt % of NCs in chlorobenzene. Solutions of F_4-TCNQ (Aldrich) with different concentrations were also prepared in the Ar atmosphere by adding the required amount of F_4-TCNQ to chlorobenzene. Dispersions of Si NCs with different amounts of F_4-TCNQ were then obtained by mixing appropriate quantities of F_4-TCNQ solutions with the Si NCs dispersions.

For electrical measurements, dispersions of Si NCs doped with F_4-TCNQ were spin-coated onto flexible polyimide substrates (Kapton, Dupont) with an interdigit Au contact grid structure consisting of 100 fingers of 2 mm length and 10 μm spacing, resulting in thin films of H-terminated Si NCs containing different concentrations of F_4-TCNQ molecules. Bottom-gate FETs were fabricated using a highly p-doped silicon wafer covered with a 50 nm thick silicon nitride gate dielectric as a substrate. An interdigit Au electrode structure consisting of 50 fingers of 2 mm length and 20 μm spacing was patterned by photolithography and thermal evaporation on top of the substrate for source and drain contacts. Afterward, FET devices were fabricated by spin-coating the Si NC doped dispersions onto the substrates. All measurements were carried out in the dark inside the same Ar-purged glovebox where the samples were prepared. Electron paramagnetic resonance (EPR) measurements were performed at room temperature in a continuous-wave Bruker spectrometer mounted with a X-band microwave bridge driven in absorption mode. In the EPR measurements, a lock-in amplifier was used with a magnetic field modulation of 100 kHz, resulting at low microwave powers in unsaturated absorption-derivative signals with intensity proportional to the square root of the microwave power, as thoroughly verified by microwave power series experiments. The spin-density measurements were calibrated using a diphenyl-picrylhydrazyl reference, magnetic field values were measured using a nuclear magnetic resonance Teslameter, and the microwave frequency was measured with a frequency counter. EPR samples were prepared inside a Ar-purged glovebox by inserting into EPR sample tubes (Suprasil quartz) a known volume (typically 100 μL) of Si NC dispersion containing different amounts of F_4-TCNQ, followed by drying of the solvent. Afterward, the open end of the quartz tubes was sealed also inside the glovebox to eliminate exposure of the samples to air during measurements. All samples within each series, including reference samples containing only F_4-TCNQ, were prepared in parallel and under the same conditions.

Theoretical. Quantum chemical calculations of disordered NC networks have been hampered for several reasons. Possibly the most important reason relates to the lack of translational symmetry across the networks, and hence to the sheer size of the problems involved. Any progress therefore has to rely upon bold simplifications, especially with regard to the size and geometry of the model. Hence, a common approach is to limit the problem to a particular region of interest, either by (i) using finite boundary conditions,[70,76] or by (ii) adopting a periodic slab-, wire-, or particle-in-a-box approach,[77−79] hoping that within such a limited region the model is still able to adequately capture the electronic local density of states. In such supercell calculations, it is also common to impose a sufficiently large vacuum space to separate the structure replicas, and by this way to mitigate unwanted periodicity effects.[80] The methods just described usually aim at studying a single nanostructure, eventually interacting with dopants, adsorbants, surfactants, and other agents. Unfortunately, the resemblance that such models bear to a NC solid, regarding the chemical environment of atoms, steric hindrance, or long-range electrostatics, may however be unsatisfactory.

dx.doi.org/10.1021/nl500932q | *Nano Lett.* 2014, 14, 3817−3826

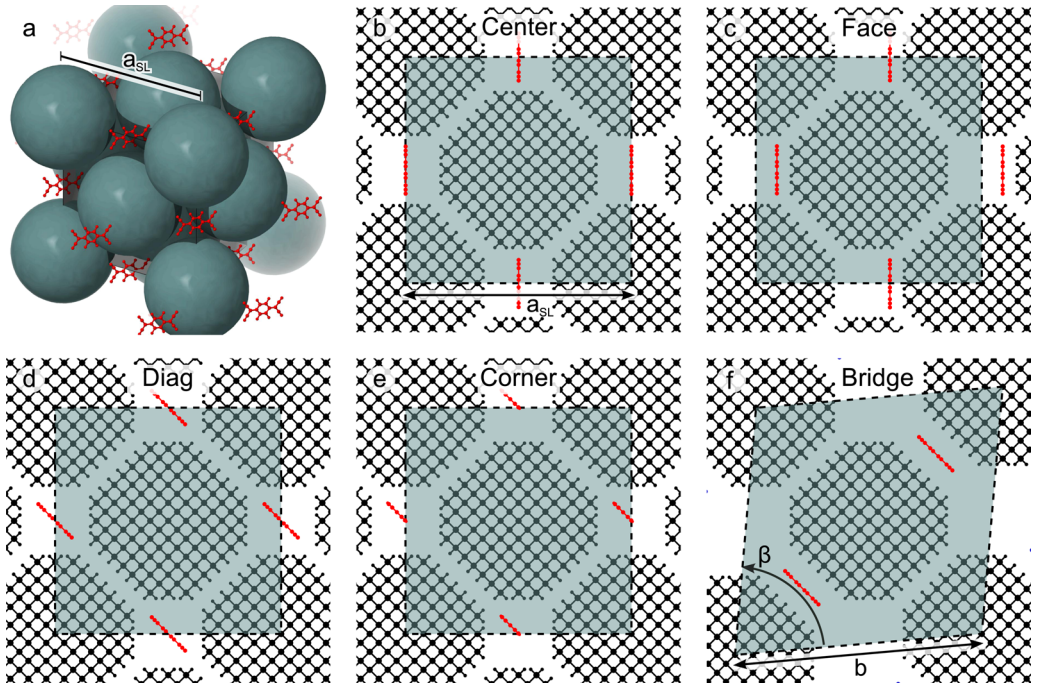

Figure 3. Configurations considered in the calculations of doped Si NC SLs. (a) Three-dimensional view of an fcc SL of Si NCs (large spheres) doped with F_4-TCNQ molecules (red). (b) fcc SL with a void-centered molecule with its plane aligned along the ⟨100⟩ direction of the Si NCs, (c) fcc SL with a molecule in the void, but adsorbed on the Si NC surface, (d) fcc SL with a void-centered molecule with its plane aligned along the ⟨110⟩ direction of the Si NCs, (e) fcc SL with a molecule close to the "corner" made by two adjacent NCs, and (f) monoclinic SL with a molecule placed between two adjacent NCs. The labeling scheme adopted for each structure is shown on top of each inset.

Here, we pack NC arrays into a periodic solid with minimal vacuum fraction and explore this avenue as a better description of NC thin films. For instance, while the calculated energy gap of a vacuum-surrounded Si NC with a diameter of 2 nm (3 nm) is about 3.1 eV (2.5 eV), the energy gap of a face-centered cubic (fcc) superlattice of identical NCs is only approximately 2.0 eV (1.8 eV). This results from Coulomb screening effects in the calculation of charged NC^+ and NC^- (to obtain the quasiparticle gap), which in the case of a packed superlattice are effectively stronger than in a particle-in-a-box-like calculation. This is very significant if we want to understand the energy level structure of a NC solid, as it is the case of the present work. Moreover, we note that the results presented in this work that relate the changes in charge transport of NC films to the molecule/NC electronic coupling involve a rather local description of the interfacial electronic density of states, energy levels, and local polarizations. Such properties are not expected to differ substantially whether the NCs are arranged randomly or in a periodic superlattice. Therefore, the periodic superlattice model is certainly a trustworthy way of predicting the properties of a real NC film, which is more realistic when compared to a particle-in-a-box approach.

Electronic structure calculations were carried out using a density functional code (AIMPRO[81,82]) along with the local spin density approximation (LSDA) for the exchange and correlation potential.[83] Core states of Si, N, F, and C atoms were replaced by the pseudopotentials of Hartwigsen, Goedecker, and Hutter,[84] while valence states were expressed as linear combinations of atom-centered Cartesian Gaussian 44G* contractions, comprising 5 functions for H atoms (including p-type polarizations) and 13 functions for Si, C, N, and F atoms (including d-type polarizations). The charge density and potential terms were Fourier-transformed using plane waves with a cutoff energy E_{cut} = 200 Hatree, and the Brillouin-zone was sampled at the Γ point.

Nearly spherical Si NCs with 347 silicon atoms were produced with a perfect crystalline core and surfaces fully saturated by hydrogen ($Si_{317}H_{172}$). Periodic boundary conditions were imposed across an fcc lattice to form an SL of Si NCs (one NC per unit cell). The SL vectors were $(110)a_{SL}/2$, $(101)a_{SL}/2$, and $(011)a_{SL}/2$ with a_{SL} being the edge length of the conventional cubic supercell. Such an arrangement is shown in Figure 3a, where the Si NCs are represented as large packed spheres. After minimizing the energy of the pristine SL with respect to the atomic structure and lattice spacing, we obtained an average Si−Si bond length $\overline{r}_b$ = 2.332 ± 0.067 Å, a SL unit cell length a_{SL} = 3.34 nm (Figure 3a), and an effective NC diameter[85] d_{NC} = 2.28 nm. Introduction of a F_4-TCNQ molecule at the cube-centered octahedral void of the SL led to a minute increase of a_{SL} (0.1−0.6%) and to a negligible impact on the NC atomic positions. Figure 3a provides a view of the molecules (shown in red) within the SL. In order to facilitate a direct comparison between different SL/molecule structures, the spacing a_{SL} = 3.34 nm of the pristine SL was adopted for all cubic SLs doped with F_4-TCNQ molecules, shown in Figure 3b−e. In one of the configurations investigated, F_4-TCNQ sits right between two neighboring NCs (Figure 3f). Unlike the other structures, such location induces a distortion to the host SL. We allowed the lowering of the SL symmetry down to monoclinic by letting SL parameters b and β, as represented in Figure 3f, to vary freely in order to minimize the total energy. Other SL distances and internal angles were equal to a_{SL} = 3.34 nm and 90°, respectively.

Results and Discussion. Figure 4 shows the dark current−voltage (I−V) characteristics recorded for films of Si NCs (d_{NC} = 15.7 nm) spun onto flexible polyimide substrates using Si NC

dx.doi.org/10.1021/nl500932q | Nano Lett. 2014, 14, 3817−3826

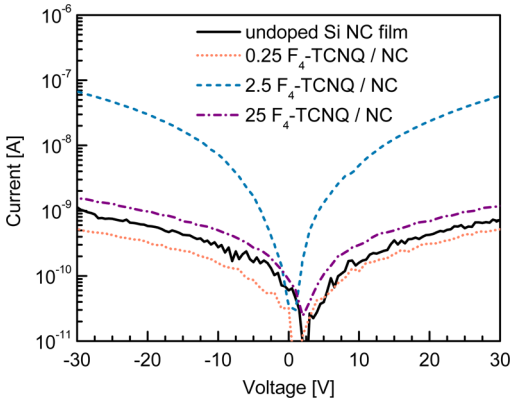

Figure 4. Current–voltage characteristics of Si NC films processed from solutions with different concentrations of F_4-TCNQ.

inks containing different concentrations of F_4-TCNQ. The I–V curve recorded for the layer with the lowest F_4-TCNQ concentration, that is, 0.25 molecules per Si NC (hereafter denoted as molecules/NC) is quite similar to that observed for the undoped Si NC film. Remarkably, an enhancement of the current by about 2 orders of magnitude is observed when the concentration of F_4-TCNQ is increased to 2.5 molecules/NC. As the F_4-TCNQ concentration is further increased, a decrease in the current is observed (see dashed–dotted line in Figure 4).[86] We have reproduced this experiment several times using different NC solutions, for example, made of Si NCs with different sizes and from different NC growth batches. The qualitative behavior of the I–V curves as a function of F_4-TCNQ concentration was however consistently the same in all cases. The data obtained from three experimental doping series are exemplarily shown in Figure 5. Here we represent the ratio

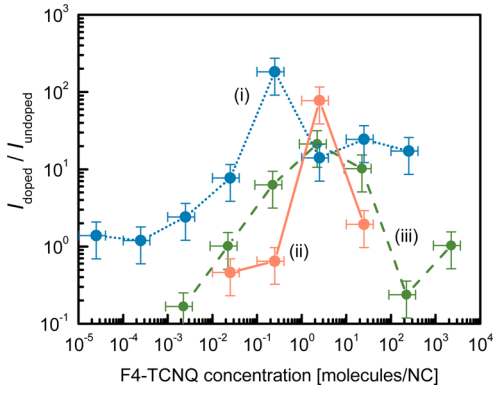

Figure 5. Evolution of the current ratio $I_{doped}/I_{undoped}$ at V = +30 V as a function of F_4-TCNQ concentration for films of Si NCs with (i) d_{NC} = 4.2 nm, (ii) d_{NC} = 15.7 nm, and (iii) d_{NC} = 17 nm.

between the current measured for F_4-TCNQ doped films (I_{doped}) to the current measured for the corresponding undoped layers ($I_{undoped}$) as a function of the F_4-TCNQ concentration. The maximum current increase was consistently of the order of 10^2 for a critical molecule concentration in the range of 10^{-1}–10^1 molecules/NC. From all data obtained, we cannot distinguish any clear dependence of this critical concentration on the NCs size. Thus, the observed range of critical concentrations should be due to other factors such as differences in the NCs (other than mean size) used in different experiments and/or variations in the distribution and configuration of F_4-TCNQ molecules within the films. We should note at this point that it is rather unlikely that the observed increase in conductance for doped films is due to differences in the morphology of these films. If we compare the size of the F_4-TCNQ molecules with the size of the NCs (the area of (planar) F_4-TCNQ molecules (~0.4 nm^2) is several orders of magnitude smaller than the surface area of the NCs (50–900 nm^2)), we conclude that the F_4-TCNQ molecules cannot influence the morphology of the films for the F_4-TCNQ concentrations at which the electrical activation is observed. The morphology of the doped and undoped films should be rather similar, because these have all been spin-cast under the same conditions from solutions with equal concentration of NCs. This conclusion is confirmed from scanning electron microscopy images (see Supporting Information), where no difference in the films' morphology can be seen for different F_4-TCNQ concentrations. Thus, the electrical activation of the films is most likely due to changes introduced in the electronic structure of the films by the F_4-TCNQ molecules.

Solution-processed NC FETs fabricated with Si NCs have been reported only recently.[71,72] Holman et al. fabricated Si NC FETs by using NCs which were synthesized in a silane plasma, transferred into solution and cast as thin films.[72] The devices exhibited n-type behavior with an estimated field-effect electron mobility of the order of 10^{-6}–10^{-5} cm^2 V^{-1} s^{-1}, and their output characteristics displayed the behavior expected for thin-film FETs. On the other hand, Weis et al.[71] reported nonlinear space-charge-limited current characteristics over the whole drain-source voltage range for similar devices. We have tested the applicability of the F_4-TCNQ-induced electrical activation of the Si NC films in solution-processed Si NC FETs. Figures 6

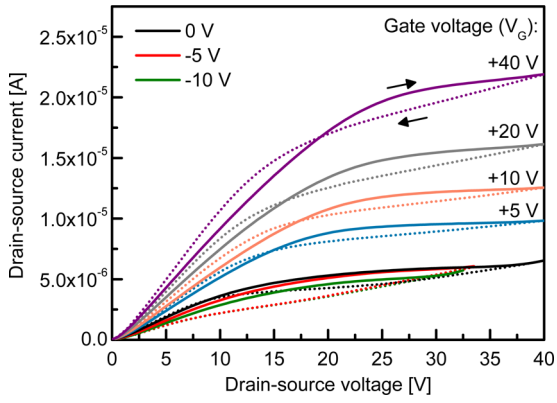

Figure 6. Drain-source current I_{DS} versus drain-source voltage V_{DS} characteristics recorded at different gate voltages V_G for a FET made of a 15.7 nm Si NCs film doped with F_4-TCNQ at a concentration of 2.5 molecules/NC. Solid and dotted lines correspond to scans in the forward and reverse directions, respectively.

and 7 show the drain-source current (I_{DS}) versus drain-source voltage (V_{DS}) characteristics for Si NC FETs doped with F_4-TCNQ at concentrations of 2.5 and 25 molecules/NC, respectively. These devices have been deposited using the same Si NC solutions and under the same deposition conditions as the corresponding films (d_{NC} = 15.7 nm) in Figure 5. In this experimental doping series, a F_4-TCNQ concentration of 2.5 molecules/NC is the critical value at which the current ratio $I_{doped}/I_{undoped}$ is maximized, whereas for a concentration of 25 molecules/NC $I_{doped}/I_{undoped}$ is again close to 1. Figures 6 and 7 show a well pronounced modulation of I_{DS}

dx.doi.org/10.1021/nl500932q | Nano Lett. 2014, 14, 3817–3826

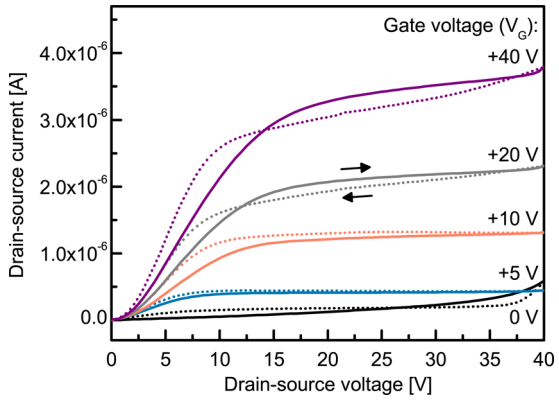

Figure 7. Drain-source current I_{DS} versus drain-source voltage V_{DS} of a Si NC (d_{NC} = 15.7 nm) FET doped with F_4-TCNQ at a concentration of 25 molecules/NC. Solid and dotted lines correspond to scans in the forward and reverse directions, respectively.

by application of a gate voltage V_G on both devices. The I_{DS}–V_{DS} characteristics is typical of thin-film FETs with a linear regime at small voltages followed by a saturation at higher V_{DS}. These data also clearly show that both devices exhibit n-type nature, at variance with findings that F_4-TCNQ is a p-type dopant in several materials (see, for example, refs 87 and 88, and references therein). We should also note that the observed critical behavior of $I_{doped}/I_{undoped}$, shown in Figure 5, is not compatible with the typical behavior of F_4-TCNQ-induced p-type doping, where donated free-carriers increase continuously with the F_4-TCNQ concentration. Below we will demonstrate that for the present system promotion of holes to the NC valence states induced by F_4-TCNQ is unlikely to take place at room temperature.

Our undoped or lightly doped Si NC FETs (for which no significant enhancement of $I_{doped}/I_{undoped}$ was observed) show no gating behavior. The observation of the typical FET behavior shown in Figures 6 and 7 enabled us to extract the field-effect electron mobility μ in the linear regime. A mobility of $\mu = 4 \pm 1 \times 10^{-5}$ cm^2 V^{-1} s^{-1} was obtained for the device with F_4-TCNQ doping of 2.5 molecules/NC. This is above the range of values of 10^{-6}–10^{-5} reported so far for the best solution-cast Si NC FETs.[71,72] For the device with [F_4-TCNQ] = 25 molecules/NC we obtain a mobility of $\mu = 2 \pm 1 \times 10^{-5}$ cm^2 V^{-1} s^{-1}. As opposed to the large hysteresis reported previously for Si NC FETs,[71,72] our devices show fairly small hysteretic effects.

To gain further insight into the origin of the electrical activation of the NC films with F_4-TCNQ, we performed first-principles calculations on undoped and doped Si NC periodic SLs. There are in principle many alternatives to accommodate a molecule within the intersticialcies of the Si NC SL. We had thus to consider different structures that, although limited in number, had to be diverse enough so that we could assess trends and general properties. We tested a total of five different structures shown in Figure 3b–f. These are abstractions of the actual structures that were fully relaxed (all atoms were displaced along the forces acting upon them with the help of a conjugate gradient algorithm) with the only constraints being those already referred above, imposed to the SL vectors. Among the structures, those in Figure 3b–e have the F_4-TCNQ molecules located at the octahedral voids of the fcc SL, while in the one shown in Figure 3f the molecule was placed right between two adjacent NCs. Here, the lattice parameters b and β that minimized the energy per supercell were b = 3.49 nm and β = 85.2°. No significant changes to the Si–Si bond lengths and Si NC diameter were found when comparing to the results from the perfect cubic SL.

For practical reasons, configurations in Figure 3 are labeled as Center (b), Face (c), Diag (d), Corner (e), and Bridge (f). A particular state of the molecule is hereafter referred to as F_4-TCNQ^q_c, with q representing a charge state (0, − or =) and c is one of the above configurations. We found F_4-TCNQ$^0_{Face}$ to be the lowest energy configuration, just 0.1 eV below F_4-TCNQ$^0_{Diag}$. The F_4-TCNQ$^0_{Center}$ and F_4-TCNQ$^0_{Corner}$ structures are about 0.7 eV above the F_4-TCNQ$^0_{Face}$ configuration. F_4-TCNQ$^0_{Face}$ maximizes the number of N–H and F–H bridge bonds with the hydrated Si surface, and this is possibly why this structure is the most stable configuration.[70]

Knowing that F_4-TCNQ is considered to be a p-type surface dopant in some materials,[87,88] we have to find out why these molecules behave differently when introduced in a Si NC network. We know from previous density functional calculations that adsorption of a F_4-TCNQ molecule to the surface of a Si NC leads to the appearance of an empty hybrid state, largely inheriting the b_{2g}-character of the lowest unoccupied molecular orbital (LUMO) of the isolated molecule.[70] This state lies just above the (also hybrid) highest occupied molecular orbital (HOMO) mostly localized on the NC,[70] and leads to a partial displacement of the topmost valence electrons from the NC to the molecule (slightly depending on the size of the NC and molecule adsorption site). Such a local polarization has also been reported when the molecule is adsorbed on insulating surfaces[89] and polymers.[88] Inspection of the Kohn–Sham states from our calculations reveals an identical behavior when the molecule is placed in a Si NC SL. That is, although F_4-TCNQ is able to polarize the NC surface, the LUMO of the doped system is mostly localized on the molecule, which is left essentially unoccupied. Effective p-type doping of the NCs could only take place in the presence of sufficient energy (for instance thermal) to promote an electron from the hybrid HOMO (mostly overlapping the NC) to the hybrid LUMO (mostly overlapping the molecule) and then to separate the just produced F_4-TCNQ$^-$-NC$^+$ electron–hole pair into uncorrelated NC$^+$ and F_4-TCNQ$^-$ ions. To look at this possibility in detail we calculated the electronic levels of F_4-TCNQ-doped SLs from total energies. This was accomplished by comparing ionization potentials and electron affinities of doped SLs (I_D and A_D, respectively) with identical quantities calculated for undoped SLs (I_U and A_U).[90] Here, I_U and A_U are representative of the valence band top and conduction band bottom energies of the Si NC, respectively, and their difference, which is $E_{g,QP} = A_U - I_U$ = 2.12 eV, is the quasi-particle gap energy. The results of the electronic level calculations are summarized in Figure 8. Here we find that, irrespectively of its configuration, the molecule is always responsible for the introduction of acceptor levels. When the molecule is less confined (F_4-TCNQ$_{Center}$ and F_4-TCNQ$_{Face}$) the (−/0) levels are shallower (0.1–0.4 eV above the valence band top). This trend results from Coulomb repulsion between the electron trapped at F_4-TCNQ$^-$ and the valence electrons from adjacent NCs. Despite the introduction of acceptor levels, the resulting range of energies clearly indicate that thermal excitation of holes from the molecules to adjacent NCs with subsequent electron–hole separation is unlikely to take place at room temperature. In fact, considering that the theoretical band gap of the calculated superlattices (2.12 eV) is considerably larger

dx.doi.org/10.1021/nl500932q | Nano Lett. 2014, 14, 3817–3826

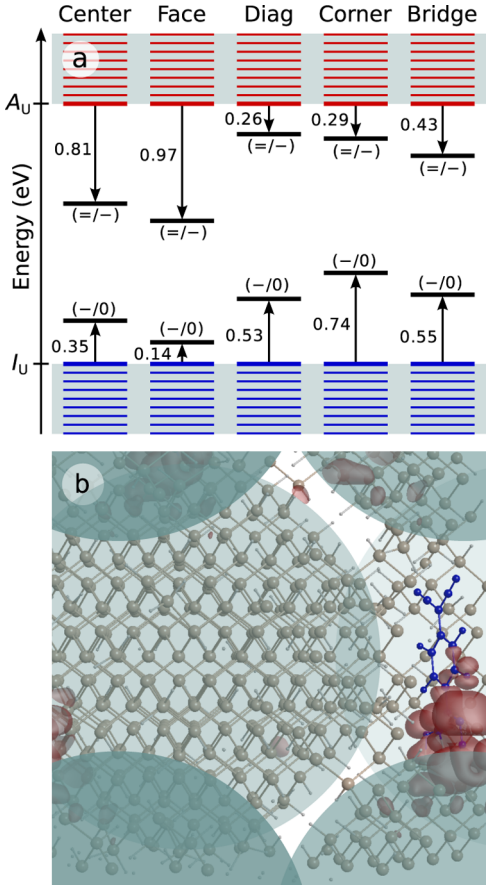

Figure 8. (a) Calculated (−/0) and (=/−) acceptor levels (black horizontal lines) of F_4-TCNQ molecules in a Si NC SL. Arrows are labeled with energy differences with respect to the ionization potential (I_U) and electron affinity (A_U) energies of the undoped SL. SL band energies are represented as blue (bottom) and red (top) horizontal lines. (b) Electron density isosurface (red) of the HOMO of F_4-$TCNQ^{=}_{Corner}$ (blue). Circles enclosing overlapping individual NCs are for eye guidance purposes.

than the energy band gap of the NCs used in the experiments (1.1−1.4 eV) and given the known underestimated correlation energies that result from the LSDA, it is expected a deviation between calculated acceptor state energies and the corresponding energies in the real samples. This deviation should be about the same with respect to the smallest (d_{NC} = 4.2 nm) and to the largest (d_{NC} = 17 nm) NCs used in the experiments if we consider the small offset between the band edges of the smallest and the largest NCs, roughly corresponding to half of the band gap difference, that is, about 0.15 eV, and the relatively larger dispersion of the energy levels obtained from the calculations. Here, the band gap of the smallest NCs corresponds to the value reported by Anthony et al.[68] for similar NCs with the same diameter and the band gap of the largest NCs corresponds to bulk silicon. Therefore, the first acceptor levels of the molecules in the real films are most likely to lie in the upper half of the band gap. We note that this conclusion is not incompatible with recent suggestions of p-type surface conductivity in Si nanowires (NWs) covered with several layers of F_4-TCNQ molecules.[91] Under such heavy doping conditions, a degenerate doping regime is most likely to occur with the formation of a surface dopant band mixed with the valence states of the NWs. A strong indication that the NW/dopant interface was actually metallic lays on the lack of a clear p-type gating behavior on the FETs made under such conditions.[91]

Interestingly, the calculations indicate that F_4-TCNQ molecules also introduce a second acceptor level within the SL band gap (see Figure 8a). For some of the configurations, the (=/−) electron trap is located within less than 0.3 eV from the bottom of the conduction band. Considering the above-mentioned underestimation of correlation effects, both (−/0) and (=/−) acceptor states are expected to raise the (unoccupied) local density of states near the conduction band energy at the inter-NC free space, thus offering additional paths for transport of electrons injected into the NC network. The large correlation energy that separates the first and second acceptor levels of the order the bulk Si band gap (∼1 eV) is a direct consequence of the strong localization of the acceptor states. The LUMO state of the isolated F_4-$TCNQ^0$ molecule is mostly localized at the nitrogen end atoms and on the carbon ring. Coulomb repulsion between electrons eventually trapped at the molecule and those at the NC valence is then expected to raise the acceptor levels further up in the band gap. This should be most prominent when the referred atomic species are closest to the film inner surface. Among all structures, F_4-$TCNQ_{Corner}$ and F_4-$TCNQ_{Diag}$ are closer to these conditions, and they are good candidates to introduce levels that could resonate with the LUMO of adjacent NCs. The proximity of the acceptor levels to the conduction band states of the NC solid suggests that electrons trapped at F_4-TCNQ molecules could easily hop to the LUMO of a neighboring NC. Overall, the acceptor states raise the (unoccupied) local density of states near the bottom of the conduction band at the inter-NC free space, thus offering additional paths for transport of electrons injected into the NC network. The depth of the (−/0) and (=/−) levels shown in Figure 8a, including those closer to the conduction band of the SL, is somewhat large when compared to the thermal energy k_BT at room temperature. However, one should mind that in addition to the underestimated correlation effects mentioned above and to the smaller band gaps of the NCs used in the experiments, the presence of an electric field, the fast thermal motion of the molecules at room temperature, or even small reconfigurations upon charge capture and emission processes, may provide in the real samples a better level alignment with conduction band states, stronger wave function overlap, and therefore the right conditions for electron transfer between molecular and empty NC levels. We note that while the more loose F_4-$TCNQ^{=}_{Center}$ and F_4-$TCNQ^{=}_{Face}$ structures show a HOMO state that resembles that of the free molecule, the HOMO of F_4-$TCNQ^{=}_{Diag}$ and F_4-$TCNQ^{=}_{Corner}$ configurations hybridize considerably with the NC states. This effect is clearly demonstrated in Figure 8b for F_4-$TCNQ^{=}_{Corner}$, implying that this type of molecular configurations could actually be responsible for the observed improvement in the electrical performance of the films.

Further experimental evidence for the resonant alignment between F_4-TCNQ-related acceptor states and LUMO states of the NCs and for the fact that F_4-TCNQ is not a p-type dopant in Si NC films is provided by EPR spectroscopy. In Figure 9a are shown the EPR spectra recorded for NC samples doped with different concentrations of F_4-TCNQ. For the undoped NCs, an EPR signal with zero crossing at g = 2.0050 is observed [spectrum (i)], which is associated with Si dangling bond defects that are typically present in Si NCs due to imperfect surface passivation.[61,69] From the intensity of this signal we estimate a defect density of approximately 0.02 defects per NC.

dx.doi.org/10.1021/nl500932q | Nano Lett. 2014, 14, 3817−3826

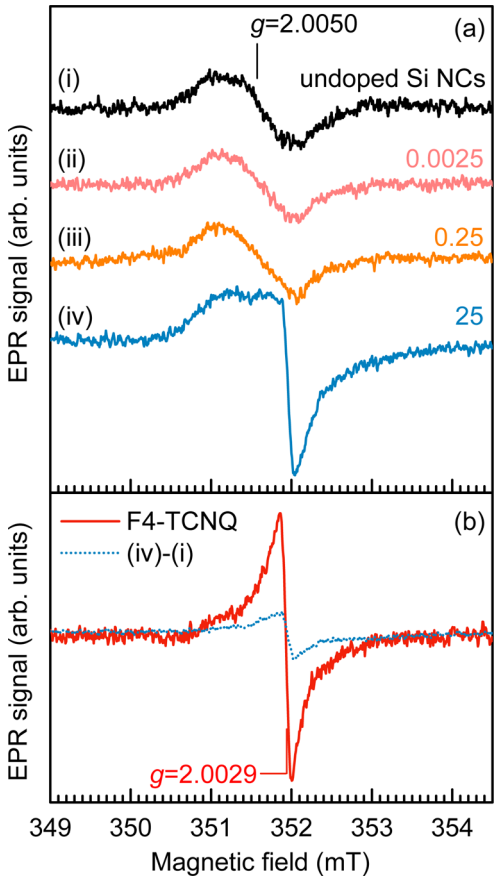

Figure 9. (a) EPR spectrum recorded for a sample of (i) undoped Si NCs together with spectra recorded for NCs samples doped with F_4-TCNQ at concentrations of (ii) 0.0025, (iii) 0.25, and (iv) 25 molecules/NC. In (a) the EPR signal intensity is normalized to the mass of NCs in each sample. (b) Comparison between the EPR spectrum recorded for a F_4-TCNQ reference sample and the result of the subtraction between spectra (iv) and (i) shown in (a). Here, the EPR signal intensity is normalized to the mass of F_4-TCNQ in each sample.

The EPR spectra of NC samples doped with F_4-TCNQ are essentially the same as that of the undoped NCs for the concentrations of 0.0025 and 0.25 molecules/NC, but for the higher concentration sample (25 molecules/NC) an additional signal can be distinguished [spectrum (iv)]. The data confirms that the (−/0) level of F_4-TCNQ lies in the upper half of the band gap. This conclusion stems from the fact that the (0/+) donor level of Si dangling bonds is located 0.3−0.5 eV above the valence band.[92,93] If the first acceptor level of F_4-TCNQ was located below the donor level of the dangling bonds, that is, ∼ 0.5 eV above the valence band top, a decrease in the EPR signal associated with Si dangling bonds (neutral state) should have been observed with increasing concentration of F_4-TCNQ. This is in clear contrast with our observations. As a matter of fact, the density of paramagnetic dangling bonds (neutral) revealed by EPR measurements is rather independent of the F_4-TCNQ concentration; see Figure 9. In Figure 9b, we compare the EPR spectrum measured for a F_4-TCNQ reference sample with the result obtained from subtracting the spectrum of the undoped NCs [spectrum (i)] to the spectrum of the F_4-TCNQ-doped sample with 25 molecules/NC [spectrum (iv)]. For the F_4-TCNQ reference sample, a signal due to F_4-TCNQ$^-$ centered at g = 2.0029 is revealed,[94,95] which results from the persistent formation of F_4-TCNQ anions in F_4-TCNQ samples.[94,95] From the EPR intensity, we estimate a density of F_4-TCNQ anions in the reference sample of $\sim 3 \times 10^{-4}$ anions/F_4-TCNQ. A 6-fold decrease of the F_4-TCNQ anion signal is observed for the NCs sample doped with F_4-TCNQ; see dotted blue spectrum in Figure 9b. We should note that the F_4-TCNQ reference sample and the sample of Si NCs doped with F_4-TCNQ (25 molecules/NC), which were prepared in parallel and under the same experimental conditions, contain nearly the same amount of F_4-TCNQ and differ only on the NC content. From the EPR data it becomes also clear that the F_4-TCNQ is not a p-type dopant of Si NCs. If that was the case, one should have observed an increase of the amount of F_4-TCNQ anions in the F_4-TCNQ-doped NCs with respect to the F_4-TCNQ reference sample, which is in contrast with our observations; see Figure 9b. While the EPR data clearly show that the first acceptor state of the F_4-TCNQ molecules lies in the upper half of the band gap and that the molecules are not p-type dopants of the Si NCs, it also allow us to infer that the acceptor levels resonate with conduction band states of the NC solid. The characteristics of our thin-film transistors demonstrates that the undoped Si NC films are effectively n-type, as also observed in previous studies.[71,72] If the acceptor states of the F_4-TCNQ were deep below the conduction band bottom of the Si NC, one would expect the high lying electrons from the n-type Si NCs to be trapped at the F_4-TCNQ molecules, leading to a markedly higher amount of F_4-TCNQ anions in the F_4-TCNQ-doped sample when compared to the reference sample. This again is not observed in our EPR experiments where a similar (or even a decreased) amount of F_4-TCNQ anions has been detected in the F_4-TCNQ doped samples; see Figure 9b.

We expect that an optimized concentration of molecules in the films should provide the best conditions for long-range charge transport when (i) it is high enough to introduce the necessary amount of extra intermediate states but also (ii) low enough to prevent an excessive accumulation of fixed charges at molecule-related (−/0) and (=/−) states that would impair charge transport due to Coulomb repulsion. In our films, the optimum critical concentration is in the range 10^{-1}−10^{1} molecules/NC, which spans the concentration of 1 molecules/NC considered in the calculations.

In summary, using Si NC thin films we have shown that long-range charge transport in NC films can be strongly enhanced by doping these films with molecules with high electron affinity (F_4-TCNQ). Si NC FETs fabricated with solution-processed Si NC layers activated by F_4-TCNQ exhibit the characteristic linear regime at small drain-source voltages followed by a saturation at higher voltages, minimal hysteresis, and field-effect electron mobilities about an order of magnitude higher than in the best solution-processed Si NC devices reported so far. Density functional calculations were carried out to understand the electronics of molecule-doped NC films. We approximated the NC films to a superlattice of packed NCs doped with molecules within its interstitialcies. To the best of our knowledge, this is an original and novel approach to study the electronic structure of NC solids. The calculations demonstrate that, when populated by electrons, hybrid molecule/NC states approach (and may actually resonate with) the conduction-band states of the NC solid. This picture is supported by EPR measurements that confirm that F_4-TCNQ acceptor levels lie in the upper half of the gap and effectively edge conduction-band states of the NC solid. Such

dx.doi.org/10.1021/nl500932q | Nano Lett. 2014, 14, 3817−3826

high-lying acceptor states provide extra electronic connectivity across the NC network as the molecules effectively flatten the electronic potential barriers for electron transfer across the otherwise vacuum-filled interstitialcies of the network. This effect also accounts for the observed electron-dominated (and not hole) charge transport of the molecule-doped films.

■ ASSOCIATED CONTENT

Supporting Information

Scanning electron microscopy images of the Si NC films. This material is available free of charge via the Internet at http://pubs.acs.org.

■ AUTHOR INFORMATION

Corresponding Authors

*E-mail: (R.N.P.) pereira@wsi.tum.de; rnpereira@ua.pt.
*E-mail: (J.C.) jose.coutinho@ua.pt.

Present Address

[#]Permanent Address: School of Electrical, Electronic and Computer Engineering, Newcastle University, Newcastle Upon Tyne NE1 7RU, United Kingdom.

Notes

The authors declare no competing financial interest.

■ ACKNOWLEDGMENTS

This work was funded by FCT through Projects No. PTDC/FIS/112885/2009, No. PEst-C/CTM/LA0025/2013, and No. RECI/FIS-NAN/0183/2012-FCOMP-01-0124-FEDER-027494, by CRUP-DAAD through the Acção Integrada Luso-Alemã A-22/09, and by DFG through Projects No. GK 1240 and No. BR 1585/6. J.C. would like to acknowledge the NanoTP Cost Action ref. MP0901.

■ REFERENCES

(1) Alivisatos, A. P. *Science* **1996**, *271*, 933−937.
(2) Murray, C. B.; Norris, D. J.; Bawendi, M. G. *J. Am. Chem. Soc.* **1993**, *115*, 8706−8715.
(3) Yu, W. W.; Wang, Y. A.; Peng, X. *Chem. Mater.* **2003**, *15*, 4300−4308.
(4) Gupta, A.; Swihart, M. T.; Wiggers, H. *Adv. Funct. Mater.* **2009**, *19*, 696−703.
(5) Mangolini, L.; Thimsen, E.; Kortshagen, U. *Nano Lett.* **2005**, *5*, 655−659.
(6) Manna, L.; Milliron, D. J.; Meisel, A.; Scher, E. C.; Alivisatos, A. P. *Nat. Mater.* **2003**, *2*, 382−385.
(7) Murray, C. B.; Kagan, C. R.; Bawendi, M. G. *Annu. Rev. Mater. Sci.* **2000**, *30*, 545−610.
(8) Regulacio, M. D.; Han, M.-Y. *Acc. Chem. Res.* **2010**, *43*, 621−630.
(9) Smith, A. M.; Nie, S. *Acc. Chem. Res.* **2010**, *43*, 190−200.
(10) Reiss, P.; Protière, M.; Li, L. *Small* **2009**, *5*, 154−168.
(11) Talapin, D. V. *Chem. Rev.* **2010**, *110*, 389−458.
(12) Vanmaekelbergh, D.; Liljeroth, P. *Chem. Soc. Rev.* **2005**, *34*, 299−312.
(13) Norris, D. J.; Efros, A. L.; Erwin, S. C. *Science* **2008**, *319*, 1776−1779.
(14) Panthani, M. G.; Khan, T. A.; Reid, D. K.; Hellebusch, D. J.; Rasch, M. R.; Maynard, J. A.; Korgel, B. A. *Nano Lett.* **2013**, *13*, 4294−4298.
(15) Tisdale, W. A.; Williams, K. J.; Timp, B. A.; Norris, D. J.; Aydil, E. S.; Zhu, X.-Y. *Science* **2010**, *328*, 1543−1547.
(16) Mocatta, D.; Cohen, G.; Schattner, J.; Millo, O.; Rabani, E.; Banin, U. *Science* **2011**, *332*, 77−81.
(17) Stegner, A. R.; Pereira, R. N.; Klein, K.; Lechner, R.; Dietmueller, R.; Brandt, M. S.; Stutzmann, M.; Wiggers, H. *Phys. Rev. Lett.* **2008**, *100*, 026803.
(18) Mangolini, L.; Kortshagen, U. *Adv. Mater.* **2007**, *19*, 2513−2519.
(19) Holman, Z. C.; Kortshagen, U. R. *Nano Lett.* **2011**, *11*, 2133−2136.
(20) Shevchenko, E. V.; Talapin, D. V.; Murray, C. B.; O'Brien, S. *J. Am. Chem. Soc.* **2006**, *128*, 3620−3637.
(21) Urban, J. J.; Talapin, D. V.; Shevchenko, E. V.; Kagan, C. R.; Murray, C. B. *Nat. Mater.* **2007**, *6*, 115−121.
(22) Murray, C. B.; Kagan, C. R.; Bawendi, M. G. *Science* **1995**, *270*, 1335−1338.
(23) Ridley, B. A.; Nivi, B.; Jacobson, J. M. *Science* **1999**, *286*, 746−749.
(24) Collier, C. P.; Vossmeyer, T.; Heath, J. R. *Annu. Rev. Phys. Chem.* **1998**, *49*, 371−404.
(25) Murray, C. B.; Kagan, C. R.; Bawendi, M. G. *Annu. Rev. Phys. Chem.* **2000**, *30*, 545−610.
(26) Kim, D. K.; Lai, Y.; Diroll, B. T.; Murray, C. B.; Kagan, C. R. *Nat. Commun.* **2012**, *3*, 1216.
(27) Talapin, D. V.; Murray, C. B. *Science* **2005**, *310*, 86−89.
(28) Konstantatos, G.; Howard, I.; Fischer, A.; Hoogland, S.; Clifford, J.; Klem, E.; Levina, L.; Sargent, E. H. *Nature* **2006**, *442*, 180−183.
(29) Mcdonald, S. A.; Konstantatos, G.; Zhang, S.; Cyr, P. W.; Klem, E. J. D.; Levina, L.; Sargent, E. H. *Nat. Mater.* **2005**, *4*, 138−142.
(30) Oertel, D. C.; Bawendi, M. G.; Arango, A. C.; Bulović, V. *Appl. Phys. Lett.* **2005**, *87*, 213505.
(31) Ginger, D. S.; Greenham, N. C. *J. Appl. Phys.* **2000**, *87*, 1361−1368.
(32) Leatherdale, C. A.; Kagan, C. R.; Morgan, N. Y.; Empedocles, S. A.; Kastner, M. A.; Bawendi, M. G. *Phys. Rev. B* **2000**, *62*, 2669−2680.
(33) Gur, I.; Fromer, N. A.; Geier, M. L.; Alivisatos, A. P. *Science* **2005**, *310*, 462−465.
(34) Luther, J. M.; Law, M.; Beard, M. C.; Song, Q.; Reese, M. O.; Ellingson, R. J.; Nozik, A. J. *Nano Lett.* **2008**, *8*, 3488−3492.
(35) Liu, C.-Y.; Holman, Z. C.; Kortshagen, U. R. *Adv. Funct. Mater.* **2010**, *20*, 2157−2164.
(36) Liu, C.-Y.; Holman, Z. C.; Kortshagen, U. R. *Nano Lett.* **2009**, *9*, 449−452.
(37) Ip, A. H.; et al. *Nat. Nanotechnol.* **2012**, *7*, 577−582.
(38) Kamat, P. V. *J. Phys. Chem. C* **2008**, *112*, 18737−18753.
(39) Tang, J.; Kemp, K. W.; Hoogland, S.; Jeong, K. S.; Liu, H.; Levina, L.; Furukawa, M.; Wang, X.; Debnath, R.; Cha, D.; Chou, K. W.; Fischer, A.; Amassian, A.; Asbury, J. B.; Sargent, E. H. *Nat. Mater.* **2011**, *10*, 765−771.
(40) Hillhouse, H. W.; Beard, M. C. *Curr. Opin. Colloid Interface Sci.* **2009**, *14*, 245−259.
(41) Sargent, E. H. *Nat. Photonics* **2009**, *3*, 325−331.
(42) Salant, A.; Shalom, M.; Tachan, Z.; Buhbut, S.; Zaban, A.; Banin, U. *Nano Lett.* **2012**, *12*, 2095−2100.
(43) Lechner, R.; Wiggers, H.; Ebbers, A.; Steiger, J.; Brandt, M. S.; Stutzmann, M. *Phys. Status Solidi RRL* **2007**, *1*, 262−264.
(44) Dai, Q.; Duty, C. E.; Hu, M. Z. *Small* **2010**, *6*, 1577−1588.
(45) Rogach, A. L.; Gaponik, N.; Lupton, J. M.; Bertoni, C.; Gallardo, D. E.; Dunn, S.; Pira, N. L.; Paderi, M.; Repetto, P.; Romanov, S. G.; O'Dwyer, C.; Sotomayor-Torres, C. M.; Eychmüller, A. *Angew. Chem., Int. Ed.* **2008**, *47*, 6538−6549.
(46) Guyot-Sionnest, P. *J. Phys. Chem. Lett.* **2012**, *3*, 1169−1175.
(47) Zabet-Khosousi, A.; Dhirani, A.-A. *Chem. Rev.* **2008**, *108*, 4072−4124.
(48) Ni, T.; Nagesha, D. K.; Robles, J.; Materer, N. F.; Müssig, S.; Kotov, N. A. *J. Am. Chem. Soc.* **2002**, *124*, 3980−3992.
(49) Kovalenko, M. V.; Scheele, M.; Talapin, D. V. *Science* **2009**, *324*, 1417−1420.
(50) Lee, J.-S.; Kovalenko, M. V.; Huang, J.; Chung, D. S.; Talapin, D. V. *Nat. Nanotechnol.* **2011**, *6*, 348−352.
(51) Nag, A.; Kovalenko, M. V.; Lee, J.-S.; Liu, W.; Spokoyny, B.; Talapin, D. V. *J. Am. Chem. Soc.* **2011**, *133*, 10612−10620.
(52) Fafarman, A. T.; Koh, W.-K.; Diroll, B. T.; Kim, D. K.; Ko, D.-K.; Oh, S. J.; Ye, X.; Doan-Nguyen, V.; Crump, M. R.; Reifsnyder, D.

C.; Murray, C. B.; Kagan, C. R. *J. Am. Chem. Soc.* **2011**, *133*, 15753−15761.
(53) Koh, W.-K.; Saudari, S. R.; Fafarman, A. T.; Kagan, C. R.; Murray, C. B. *Nano Lett.* **2011**, *11*, 4764−4767.
(54) Choi, J.-H.; Fafarman, A. T.; Oh, S. J.; Ko, D.-K.; Kim, D. K.; Diroll, B. T.; Muramoto, S.; Gillen, J. G.; Murray, C. B.; Kagan, C. R. *Nano Lett.* **2012**, *12*, 2631−2638.
(55) Rosen, E. L.; Buonsanti, R.; Llordes, A.; Sawvel, A. M.; Milliron, D. J.; Helms, B. A. *Angew. Chem., Int. Ed.* **2012**, *51*, 684−689.
(56) Chung, D. S.; Lee, J.-S.; Huang, J.; Nag, A.; Ithurria, S.; Talapin, D. V. *Nano Lett.* **2012**, *12*, 1813−1820.
(57) Oh, S. J.; Berry, N. E.; Choi, J.-H.; Gaulding, E. A.; Paik, T.; Hong, S.-H.; Murray, C. B.; Kagan, C. R. *ACS Nano* **2013**, *7*, 2413−2421.
(58) Williams, K. J.; Tisdale, W. A.; Leschkies, K. S.; Haugstad, G.; Norris, D. J.; Aydil, E. S.; Zhu, X.-Y. *ACS Nano* **2009**, *3*, 1532−1538.
(59) Rafiq, M. A.; Tsuchiya, Y.; Mizuta, H.; Oda, S.; Uno, S.; Durrani, Z. A. K.; Milne, W. I. *Appl. Phys. Lett.* **2005**, *87*, 182101.
(60) Pereira, R. N.; Niesar, S.; You, W. B.; da Cunha, A. F.; Erhard, N.; Stegner, A. R.; Wiggers, H.; Willinger, M.-G.; Stutzmann, M.; Brandt, M. S. *J. Phys. Chem. C* **2011**, *115*, 20120−20127.
(61) Niesar, S.; Pereira, R. N.; Stegner, A. R.; Erhard, N.; Hoeb, M.; Baumer, A.; Wiggers, H.; Brandt, M. S.; Stutzmann, M. *Adv. Funct. Mater.* **2012**, *22*, 1190−1198.
(62) Cheng, K.-Y.; Anthony, R.; Kortshagen, U. R.; Holmes, R. J. *Nano Lett.* **2010**, *10*, 1154−1157.
(63) Cheng, K.-Y.; Anthony, R.; Kortshagen, U. R.; Holmes, R. J. *Nano Lett.* **2011**, *11*, 1952−1956.
(64) English, D. S.; Pell, L. E.; Yu, Z.; Barbara, P. F.; Korgel, B. A. *Nano Lett.* **2002**, *2*, 681−685.
(65) Yu, Y.; Bosoy, C. A.; Hessel, C. M.; Smilgies, D.-M.; Korgel, B. A. *ChemPhysChem* **2013**, *14*, 84−87.
(66) Kim, D. W.; Jang, J.; Kim, H.; Cho, K.; Kim, S. *Thin Solid Films* **2008**, *516*, 7715−7719.
(67) Kang, M. S.; Lee, J.; Norris, D. J.; Frisbie, C. D. *Nano Lett.* **2009**, *9*, 3848−3852.
(68) Anthony, R. J.; Rowe, D. J.; Stein, M.; Yang, J.; Kortshagen, U. *Adv. Funct. Mater.* **2011**, *21*, 4042−4046.
(69) Pereira, R. N.; Rowe, D. J.; Anthony, R. J.; Kortshagen, U. *Phys. Rev. B* **2012**, *86*, 085449.
(70) Carvalho, A.; Coutinho, J.; Barroso, M.; Silva, E. L.; Öberg, S.; Rayson, M.; Briddon, P. R. *Phys. Rev. B* **2011**, *84*, 125437.
(71) Weis, S.; Körmer, R.; Jank, M. P. M.; Lemberger, M.; Otto, M.; Ryssel, H.; Peukert, W.; Frey, L. *Small* **2011**, *7*, 2853−2857.
(72) Holman, Z. C.; Liu, C.-Y.; Kortshagen, U. R. *Nano Lett.* **2010**, *10*, 2661−2666.
(73) Pereira, R. N.; Rowe, D. J.; Anthony, R. J.; Kortshagen, U. *Phys. Rev. B* **2011**, *83*, 155327.
(74) Brunauer, S.; Emmet, P.; Teller, E. *J. Am. Chem. Soc.* **1938**, *60*, 309−319.
(75) Knipping, J.; Wiggers, H.; Rellinghaus, B.; Roth, P.; Konjhodzic, D.; Meier, C. *J. Nanosci. Nanotechnol.* **2004**, *4*, 1039.
(76) Chelikowsky, J. R.; Alemany, M. M. G.; Chan, T.-L.; Dalpian, G. M. *Rep. Prog. Phys.* **2011**, *74*, 046501.
(77) Du, M.-H.; Erwin, S. C.; Efros, A. L. *Nano Lett.* **2008**, *8*, 2878−2882.
(78) Cantele, G.; Degoli, E.; Luppi, E.; Magri, R.; Ninno, D.; Iadonisi, G.; Ossicini, S. *Phys. Rev. B* **2005**, *72*, 113303.
(79) Chan, T.-L.; Chelikowsky, J. R. *Nano Lett.* **2010**, *10*, 821−825.
(80) Gali, A.; Vörös, M.; Rocca, D.; Zimanyi, G. T.; Galli, G. *Nano Lett.* **2009**, *9*, 3780−3785.
(81) Briddon, P. R.; Jones, R. *Phys. Status Solidi B* **2000**, *217*, 131−171.
(82) Rayson, M. J.; Briddon, P. R. *Comput. Phys. Commun.* **2008**, *178*, 128−134.
(83) Perdew, J. P.; Wang, Y. *Phys. Rev. B* **1992**, *45*, 13244−13249.
(84) Hartwigsen, C.; Goedecker, S.; Hutter, J. *Phys. Rev. B* **1998**, *58*, 3641−3662.
(85) The radius R_{NC} of a NC with N Si atoms is calculated from that of a sphere with volume equivalent to the same number of atoms in bulk, that is, $\sqrt{3}R_{NC} = (3N/2\pi)^{1/3}\overline{r}_b$, where $\overline{r}_b$ is the average Si−Si bond length.
(86) In these curves, the current minimum seems to appear at a voltage different from $V = 0$ V. This artifact is due to the background (open circuit) current of the measurement apparatus which results in the reading of a nonzero current at $V = 0$ V. This is normally apparent when $I-V$ data with small currents are plotted in log scale and plays no role in our discussion.
(87) Chen, W.; Qi, D.; Gao, X.; Wee, A. T. S. *Prog. Surf. Sci.* **2009**, *84*, 279−321.
(88) Pingel, P.; Neher, D. *Phys. Rev. B* **2013**, *87*, 115209.
(89) Braun, S.; Salaneck, W. R. *Chem. Phys. Lett.* **2007**, *438*, 259−262.
(90) Coutinho, J.; Markevich, V. P.; Peaker, A. R.; Hamilton, B.; Lastovskii, S. B.; Murin, L. I.; Svensson, B. J.; Rayson, M. J.; Briddon, P. R. *Phys. Rev. B* **2012**, *86*, 174101.
(91) Yuan, G. D.; Ng, T. W.; Zhou, Y. B.; Wang, F.; Zhang, W. J.; Tang, Y. B.; Wang, H. B.; Luo, L. B.; Wang, P. F.; Bello, I.; Lee, C. S.; Lee, S. T. *Appl. Phys. Lett.* **2010**, *97*, 153126.
(92) Gerardi, G. J.; Poindexter, E. H.; Caplan, P. J.; Johnson, N. M. *Appl. Phys. Lett.* **1986**, *49*, 348−350.
(93) Grimmeiss, H. G.; Buchwald, W. R.; Poindexter, E. H.; Caplan, P. J.; Harmatz, M.; Gerardi, G. J.; Keeble, D. J.; Johnson, N. M. *Phys. Rev. B* **1989**, *39*, 5175−5185.
(94) Gerson, F.; Heckendorn, R.; Cowan, D. O.; Kini, A. M.; Maxfield, M. *J. Am. Chem. Soc.* **1983**, *105*, 7017−7023.
(95) Rataiczak, R. D.; Jones, M. T.; Reeder, J. R.; Sandman, D. J. *Mol. Phys.* **1985**, *56*, 65−77.